Anisotropic sub-grid scale numerical schemes for Large Eddy Simulations of turbulent flows

Georges-Henri Cottet

Anisotropic subgrid-scale numerical schemes for Large Eddy Simulations of turbulent flows

G.-H. Cottet
LMC-IMAG
Université Joseph Fourier
BP53 Grenoble Cédex 9, France

April 20, 1998

Abstract

Subgrid-scale models using anisotropic eddy-viscosity tensors are considered and used to derive new numerical schemes for Large Eddy Simulations. The derivation is based on integral representations of differential operators and directly leads to algorithms using only velocity values at grid points. The asymptotic behavior of the model near boundaries is discussed and several implementation options are described, including techniques for backscatter control which distinguish between the strain directions in the flow. A numerical validation is carried out on channel flow calculations and possible extensions of the method are outlined.

1 Introduction

The goal of subgrid-scale models in Large Eddy Simulations is to parameterize the effect of the small scales that cannot be resolved on the grid. The best-known such model is the Smagorinsky model [14] where the residual stress is modeled by a dissipation term, with a viscous length scale proportional to the filter width, to allow energy to cascade from the large scales to the small scales.

Although this model performs rather well for isotropic turbulence, it is well known that it has difficulties when applied to wall bounded flows. In particular it fails to exhibit the correct asymptotic behavior near walls where it gives too large dissipation rates. To correct this defect, damping procedures where the dissipation is explicitly inhibited near walls have been proposed and successfully implemented for wall-bounded flows [12]. This method however is difficult to extend to complex geometries.

An alternative approach, the so-called dynamic procedure, is to use the Smagorinsky model with an adaptive, space and time dependent, calculation of the coefficient. This is done by modeling the Reynolds stress at two different filter widths and expressing the difference in terms of resolved quantities. This leads to 6 integral equations for the unknown Smagorinsky coefficient. When the flow is homogeneous in at least one direction along which the coefficient is assumed to be constant, this system can be given a simple least square solution, which is then averaged in the homogeneous directions. The resulting method (the so-called global dynamic model) has allowed to obtain good agreement between low resolution LES simulations and high resolution DNS results in many flow configurations at low Reynolds number. Comparisons with experimental data at higher Reynolds numbers which so far were beyond the capacity of numerical simulations confirmed that the dynamic procedure is a valuable tool for LES computations.

For more complex flows, it has been found that the brute force solution of the integral equations could lead to locally persistent negative viscosity values, eventually resulting in unstable algorithms. The common remedy is to constrain the coefficient to be positive [6, 13]. This approach has been validated in a variety of flows and some comparisons with the global dynamic model have been made for channel flows [1], but it remains difficult to predict the impact of the positivity constraint in general flow geometries.

Our goal here is to investigate anisotropic alternatives to the Smagorinsky model. This approach is by no means new. It has indeed long been recognized that off-diagonal terms in the subgrid-scale dissipation could add some flexibility to the Smagorinsky model, improve its performance in particular in near-wall regions and stabilize its dynamic formulation. This possibility has mostly been studied through a priori testing, from the point of view of correlations based on DNS or experimental data [9, 10].

The basic equations for Large Eddy Simulations are the filtered Navier-Stokes equations

$$\frac{\partial \overline{u}_i}{\partial t} + (\overline{\mathbf{u}} \cdot \nabla)\overline{u}_i + \frac{\partial \overline{p}}{\partial x_i} - \nu \Delta \overline{u}_i = -\frac{\partial \tau_{ij}}{\partial x_j} \tag{1}$$

$$\text{div}\,\{\overline{\mathbf{u}}\} = 0 \tag{2}$$

where $\overline{\mathbf{u}} = (\overline{u}_i)$ and $\overline{p}$ are the resolved velocity and pressure, ν is the kinematic viscosity and (τ_{ij}) is the subgrid-scale tensor

$$\tau_{ij} = \overline{u_i u_j} - \overline{u}_i \overline{u}_j.$$

Here and throughout this paper we adopt the convention of implicit summation of repeated indices. Our starting point will be the following model:

$$\tau_{ij} \simeq C \Delta^2 D_{ik}\overline{\mathbf{u}} D_{jk}\overline{\mathbf{u}} \tag{3}$$

where $D_{ik}\overline{\mathbf{u}} = \frac{\partial u_i}{\partial x_k}$ and Δ is the filter width. We wish to stress the fact that our interest here is not to discuss the validity of (3) from the modeling point of view, but rather from the

implementation and efficiency point of view. Although the original derivation of (3) [8] as a leading order expansion for the Leonard stress $L_{ij} = \overline{\overline{u}_i \overline{u}_j} - \overline{\overline{u}}_i \overline{\overline{u}}_j$ clearly does not account for the full subgrid-scale tensor, we merely view it here as the simplest possible anisotropic alternative to the Smagorinsky model, with the required symmetry with respect to the indices i and j.

One difficulty associated to the subgrid-scale model (3), sometimes called the gradient model, is that it induces backscatter as well as dissipation. It thus requires some clipping. The clipping procedures proposed in the litterature consist in ignoring the subgrid-scale term at all points where its contribution to energy balance would be positive. It is then in general recognized that the model is not dissipative enough. This is why it is often complemented by a Smagorinsky term in so-called mixed models. The pitfall of this is of course that one loses the potential gains offered by the original anisotropic form of the model over the Smagorinsky model. For a systematic comparison of the gradient and mixed models with the Smagorinsky model in shear layers we refer to [15].

We believe that the difficulties experienced with the gradient model originate in the fact that its clipped version proposed so far do not retain its anisotropy. It is actually very likely that (3) contains both dissipation and backscatter at every point along different strain directions. In a clipped model, it is therefore important to be able to distinguish between these directions. In this paper we propose discretization formulas for (3) which can be implemented in any grid-based numerical method and allows to determine easily backscatter and dissipation directions at every grid point, enabling sharp clipping procedures.

Numerical tests concerning isotropic turbulence, which are presented elsewhere [3], indicate that this approach indeed overcomes the difficulties above mentioned and yields models which, even in this case, are superior to the Smagorinsky model. Since the purpose of anisotropic models is principally to improve the Smagorinsky model in near-wall regions, to illustrate the

properties of our numerical models we have chosen to focus here on Large Eddy Simulations of channel flows, where, as we already mentioned, it is well-known that the Smagorinsky model fails in absence of ad-hoc damping or dynamic coefficient calculations.

An outline of the paper is as follows. In section 2, we use integral approximations to derive our numerical schemes. We check then that they exhibit an asymptotic decay in the near wall region which is consistent with (3). This rate, if it does not match the dynamic model's rate, definitely distinguishes the anisotropic from the Smagorinsky model. We show that the decay rate can be further improved if the integral formula is implemented on a grid refined in the wall normal direction. In this case, the integral formula departs from the original model (3); it corresponds to a subgrid-scale model which we believe is more appropriate to a filtering of the Navier-Stokes equations with a variable-size filter. We then present our backscatter control strategy which distinguishes between directions of diffusion and anti-diffusion in the flow. As a side remark we propose an interpretation of a vortex scheme recently derived in [2] in terms of subgrid-scale modeling for vortex methods. We also indicate how a dynamic procedure can be implemented to determine the coefficient values in the numerical method. Various implementation options are finally tested in section 3 and compared against numerical and experimental results for channel flows. Finally some conclusions are drawn in section 4 from these preliminary results and future plans for the implementation of the model are discussed.

2 Anisotropic grid formulas

The basic tool in the derivation to follow will be to use an integral representation of the differential operator appearing in the right hand side of (3) and to discretize the integrals on grid points. Throughout this section, we will assume either periodic, no-slip condition at a solid boundary or vanishing velocity at infinity, or any combination of these boundary conditions.

For the sake of simplicity we will consider incompressible flows; however we wish to point out that similar calculations, although slightly more involved, carry over to the compressible case. For notational convenience, we will drop the overbar notation for the computed quantities.

2.1 Integral formulas

Let ζ be any filter function satisfying

$$\int x_k x_l \zeta(\mathbf{x})\, d\mathbf{x} = \delta_{kl} \tag{4}$$

where $k, l \in [1,3]$, x_k denote the components of $\mathbf{x}$ and δ_{kl} is the Kronecker symbol. Such a filter can be easily designed through proper rescaling from any positive function satisfying symmetry properties (e.g. functions with spherical symmetry, or functions constructed through tensor product of one-dimensional even functions). Note that ζ is a numerical filter (or cut-off) which does not necessarily coincide with the filter underlying the derivation of the SGS model (3). In view of (4) we can write:

$$\Delta^2 D_{ik}\mathbf{u}(\mathbf{x}) D_{jk}\mathbf{u}(\mathbf{x}) = \Delta^{-3} \int D_{ik}\mathbf{u}(\mathbf{x}) D_{jl}\mathbf{u}(\mathbf{x}) (y_k - x_k)(y_l - x_l) \zeta(\frac{\mathbf{y}-\mathbf{x}}{\Delta})\, d\mathbf{y} \tag{5}$$

where we recall that the summation of repeated indices is implied. In the above formula, Δ is the filter width, which, for the time being, is assumed to be constant. By Taylor expansions of u_i and u_j around $\mathbf{x}$, this yields

$$\Delta^2 D_{ik}\mathbf{u}(\mathbf{x}) D_{jk}\mathbf{u}(\mathbf{x}) = \Delta^{-3} \left\{ \int [u_j(\mathbf{y}) - u_j(\mathbf{x})][u_i(\mathbf{y}) - u_i(\mathbf{x})] \zeta(\frac{\mathbf{y}-\mathbf{x}}{\Delta})\, d\mathbf{y} + O(\Delta^2) \right\} \tag{6}$$

Since ultimately it is the divergence of τ_{ij} that we need to model to solve the filtered Navier-Stokes equations (1), we take the divergence of (6) to obtain, after cancellation of the term involving the divergence of $\mathbf{u}$:

$$\partial_j \left[D_{ik}\mathbf{u}(\mathbf{x}) D_{jk}\mathbf{u}(\mathbf{x}) \right] \simeq A_i + B_i \tag{7}$$

where we used the notation ∂_j for $\partial/\partial x_j$ and

$$A_i = -\Delta^{-3} \int [u_j(\mathbf{y}) - u_j(\mathbf{x})] \partial_j u_i(\mathbf{x}) \zeta(\frac{\mathbf{y}-\mathbf{x}}{\Delta})\, dy$$

$$B_i = -\Delta^{-4} \int [u_j(\mathbf{y}) - u_j(\mathbf{x})][u_i(\mathbf{y}) - u_i(\mathbf{x})] \partial_j \zeta(\frac{\mathbf{y}-\mathbf{x}}{\Delta})\, d\mathbf{y}$$

It is readily seen that A_i are convective terms: if one sets $\lambda = \int \zeta(\mathbf{y})\, d\mathbf{y}$ and

$$\hat{\mathbf{u}}(\mathbf{x}) = \frac{1}{\lambda \Delta^3} \int \mathbf{u}(\mathbf{y}) \zeta(\frac{\mathbf{y}-\mathbf{x}}{\Delta})\, d\mathbf{y}$$

then A_i can be rewritten as $(\hat{\mathbf{u}} - \mathbf{u}) \nabla u_i$. It thus does not contribute to the energy balance. Since the goal of SGS models is to allow the transfer of energy between large and small scales, we will disregard this term and focus on B_i. As a result, the SGS model we end up with reads:

$$\partial_j \tau_{ij} \simeq -C\Delta^{-4} \int [u_j(\mathbf{y}) - u_j(\mathbf{x})][u_i(\mathbf{y}) - u_i(\mathbf{x})] \partial_j \zeta(\frac{\mathbf{y}-\mathbf{x}}{\Delta})\, d\mathbf{y} \tag{8}$$

The main ingredient in the above derivation was the moment condition (4). It is interesting to observe that the model (8) using a filter with vanishing second order moments would be most likely related to a subgrid-scale model of hyperviscosity type.

We have chosen above a self-contained and rather straightforward derivation of the integral formula (8). It is also possible to derive this formula through the general tools described in an abstract framework in [4]. These tools allow to handle the compressible case as well. One then obtains a formula similar to (8) complemented by a term proportional to the divergence of the velocity at the point x.

It will be important in the sequel to measure the subgrid-scale dissipation $\mathcal{D}$ resulting from our model. Multiplying both sides of (8) by u_i, we get:

$$\mathcal{D} = -C\Delta^{-4} \int [u_j(\mathbf{y}) - u_j(\mathbf{x})][u_i(\mathbf{y}) - u_i(\mathbf{x})] \partial_j \zeta(\frac{\mathbf{y}-\mathbf{x}}{\Delta}) u_i(\mathbf{x})\, d\mathbf{x}\, d\mathbf{y} \tag{9}$$

We next rewrite $u_i(\mathbf{x}) = \frac{1}{2}[u_i(\mathbf{x}) + u_i(\mathbf{y})] + \frac{1}{2}[u_i(\mathbf{x}) - u_i(\mathbf{y})]$ and we observe that, by symmetry, the first term does not contribute to the integral in the right hand side of (9). So we are left with

$$\mathcal{D} = \frac{C}{2}\Delta^{-4}\sum_j \int [u_j(\mathbf{y}) - u_j(\mathbf{x})]|\mathbf{u}(\mathbf{y}) - \mathbf{u}(\mathbf{x})|^2 \partial_j \zeta(\frac{\mathbf{y}-\mathbf{x}}{\Delta})\, d\mathbf{x}\, d\mathbf{y}$$

or, in closed form,

$$\mathcal{D} = \frac{C}{2}\Delta^{-4}\int [\mathbf{u}(\mathbf{y}) - \mathbf{u}(\mathbf{x})] \cdot \nabla\zeta(\frac{\mathbf{y}-\mathbf{x}}{\Delta})|\mathbf{u}(\mathbf{y}) - \mathbf{u}(\mathbf{x})|^2\, d\mathbf{x}\, d\mathbf{y} \tag{10}$$

2.2 Asymptotic behavior near walls

As we now show, a property which strikingly distinguishes the anisotropic model from the scalar Smagorinsky model is its behavior near walls.

Assume a smooth velocity $\mathbf{u} = (u_1, u_2, u_3)$ vanishing at $x_2 = 0$. By the continuity equation we thus have $\partial u_2/\partial x_2 = 0$ at $x_2 = 0$ and, near the wall, assuming for a sake of simplicity that all the proportionality constants are equal 1,

$$u_1 \simeq x_2, u_2 \simeq x_2^2, u_3 \simeq x_2 \tag{11}$$

To simplify the forthcoming calculation, assume that the filter has radial symmetry: $\zeta(x) = f(|x|)$. Assume further that it has compact support with unit size and that $x_2 \geq \Delta$. In view of (10), it is natural to evaluate the SGS dissipation at distance x_2 from the wall with the formula

$$\mathcal{D}(x_2) = \frac{C}{2}\Delta^{-4}\int [\mathbf{u}(\mathbf{y}) - \mathbf{u}(\mathbf{x})] \cdot \nabla\zeta(\frac{\mathbf{y}-\mathbf{x}}{\Delta})|\mathbf{u}(\mathbf{y}) - \mathbf{u}(\mathbf{x})|^2\, dx_1\, dx_3\, d\mathbf{y} \tag{12}$$

Substituting (11) into (12), we get

$$\begin{aligned}\mathcal{D}(x_2) \;=\; & \frac{C}{2}\Delta^{-4}\int \frac{1}{|\mathbf{x}-\mathbf{y}|}\Big[(x_2-y_2)(x_1-y_1) + (x_2^2-y_2^2)(x_2-y_2) + (x_2-y_2)(x_3-y_3)\Big] \\ & f'(\frac{|\mathbf{x}-\mathbf{y}|}{\Delta})|\mathbf{u}(\mathbf{y}) - \mathbf{u}(\mathbf{x})|^2\, dx_1\, dx_3\, d\mathbf{y}\end{aligned}$$

By symmetry the integrals involving the terms $(x_1 - y_1)$ and $(x_3 - y_3)$ drop out. Moreover, if $x_2 \geq \Delta$ and $|\mathbf{x} - \mathbf{y}| \leq \Delta$, we can write

$$|(x_2^2 - y_2^2)(x_2 - y_2)| = |x_2 - y_2|^2 |x_2 + y_2| \leq 3x_2 |\mathbf{x} - \mathbf{y}|^2$$

Using $|\mathbf{x} - \mathbf{y}|^2 \leq \Delta^3 |\mathbf{x} - \mathbf{y}|^{-1}$ we obtain

$$\mathcal{D}(x_2) \leq 3x_2 \, \Delta^{-1} \int \frac{|\mathbf{u}(\mathbf{x}) - \mathbf{u}(\mathbf{y})|^2}{|\mathbf{x} - \mathbf{y}|^2} f'(\frac{|\mathbf{x} - \mathbf{y}|}{\Delta}) \, dx_1 \, dx_3 \, d\mathbf{y}$$

Next, still for $|\mathbf{x} - \mathbf{y}| \leq \Delta$, $\frac{|\mathbf{u}(\mathbf{x}) - \mathbf{u}(\mathbf{y})|}{|\mathbf{x} - \mathbf{y}|}$ can be estimated, to the leading order, by $|\nabla \mathbf{u}|$, so we end up with

$$\mathcal{D}(x_2) \leq C' x_2 \Delta^2 \int |\nabla \mathbf{u}|^2 \, dx_1 \, dx_3 \tag{13}$$

The $O(x_2)$ decay of the dissipation rate is consistent with the form (3) from which our model derives. Even if it does not match the correct $O(x_2^3)$ rate, it strongly contrasts with what would result from the Smagorinsky model (since the strain rate is of the order of 1, the Smagorinsky model would give a dissipation rate of the order of $\Delta^2 |\nabla \mathbf{u}|^2$). We will see below how grid refinement can translate into an improved decay rate.

2.3 Grid implementations

In a grid-based numerical algorithm, such as the collocation method we will use in our experiments, a natural way to discretize (8) is to use the grid points as quadrature points, with the appropriate weights, for the numerical integration of the integral in the right hand side of (8). As for the filter shape and width, for practical commodity it is natural to require them to adjust to the grid geometry. This leads us to distinguish between uniform and variable-size grids.

2.3.1 The case of a uniform grid

Assume first that we are dealing with a uniform square grid, with grid size ε. An obvious choice consists in taking $\Delta = \varepsilon$ together with a radially symmetric filter $\zeta(\mathbf{x}) = f(|\mathbf{x}|)$. If one

takes for f the hat function with support of size unity, for a given grid point the integral in the right hand side of (8) extends to the 8 nearest points. If the grid is parallel to the axis, its implementation will be equivalent to the finite-difference stencil sketched in Figure 1.
Notice that, although taking only the nearest grid points may be thought as a rather crude sampling of the integrand in the integral model, this does not preclude the derivation of the model as an approximation of (3): to by-pass the quadrature error in the integral it suffices to replace the continuous moment properties (4) by the corresponding discrete properties.

2.3.2 The case of a variable-size grid

We now turn to the case of a non-uniform, but still cartesian, grid. This is the case we will have to deal with in the channel flow calculations described in the next section. To adjust to the grid, the filter has to be the tensor product of one-dimensional functions, each of these functions having a support extending to the nearest grid point in the corresponding direction. In the typical case of a wall-bounded flow and a grid refining in the wall normal direction, this results in a high aspect ratio filter. One can expect from the analysis in 2.1 that the stretching of the grid will affect the dissipation rates in the corresponding directions. This is confirmed by the following argument.

Assume that the filter ζ is built from a unique one dimensional shape ρ in all 3 directions. Let us denote by $\Delta_1(x_1), \Delta_2(x_2), \Delta_3(x_3)$ the local grid sizes in the 3 directions and set $\omega(\mathbf{x}) = \Delta_1(x_1)\Delta_2(x_2)\Delta_3(x_3)$. Natural formulas which extends (6) and (8) to this case are

$$\tau_{ij}(\mathbf{x}) \simeq \frac{C}{\omega(\mathbf{x})} \int [u_j(\mathbf{y}) - u_j(\mathbf{x})][u_i(\mathbf{y}) - u_i(\mathbf{x})]\zeta(\mathbf{x},\mathbf{y})\, d\mathbf{y} \tag{14}$$

$$\sum_j \partial_j \tau_{ij}(\mathbf{x}) \simeq \frac{C}{\omega(\mathbf{x})} \sum_j \frac{1}{\Delta_j(x_j)} \int [u_j(\mathbf{y}) - u_j(\mathbf{x})][u_i(\mathbf{y}) - u_i(\mathbf{x})]\lambda_j(\mathbf{x},\mathbf{y})\, d\mathbf{y} \tag{15}$$

where

$$\zeta(\mathbf{x},\mathbf{y}) = \rho(\frac{x_1-y_1}{\Delta_1(\mathbf{x})})\rho(\frac{x_2-y_2}{\Delta_2(\mathbf{x})})\rho(\frac{x_3-y_3}{\Delta_3(\mathbf{x})}) \ ; \ \lambda_1(\mathbf{x},\mathbf{y}) = \rho'(\frac{x_1-y_1}{\Delta_1(\mathbf{x})})\rho(\frac{x_2-y_2}{\Delta_2(\mathbf{x})})\rho(\frac{x_3-y_3}{\Delta_3(\mathbf{x})})$$

and similar formulas for λ_2, λ_3. To elucidate the differential model to which this integral formula is precisely related, it is convenient to work through change of variables. We will assume that the physical variable size grid (x_1, x_2, x_3) can be mapped to a uniform grid (ξ_1, ξ_2, ξ_3) with grid size Δ via the change of variables $\xi_i = g_i(x_i)$. With these notations, the grid spacing in the original mesh is related to Δ by the formula

$$\Delta_j(\mathbf{x}) = \Delta / g_j'(x_j)$$

We then set $\tilde{\mathbf{u}}(\boldsymbol{\xi}) = \mathbf{u}(\mathbf{x})$ and immediately get

$$D_{ik}\tilde{\mathbf{u}} D_{jk}\tilde{\mathbf{u}} = \frac{1}{|g_k'(\mathbf{x})|^2} D_{ik}\mathbf{u} D_{jk}\mathbf{u}$$

and

$$\frac{\partial}{\partial x_j}\left(\Delta_k(x)^2 D_{ik}\mathbf{u} D_{jk}\mathbf{u}\right) = \frac{\Delta^3}{\Delta_j(\mathbf{x})}\frac{\partial}{\partial \xi_j}\left(D_{ik}\tilde{\mathbf{u}} D_{jk}\tilde{\mathbf{u}}\right) \tag{16}$$

The analysis of section 2.1 applied in the $\boldsymbol{\xi}$ uniform mesh then yields

$$\frac{\partial}{\partial \xi_j}\left(D_{ik}\tilde{\mathbf{u}} D_{jk}\tilde{\mathbf{u}}\right)(\boldsymbol{\xi}) \simeq -C\Delta^{-6}\sum_j \int [\tilde{u}_j(\boldsymbol{\eta}) - \tilde{u}_j(\boldsymbol{\xi})][\tilde{u}_i(\boldsymbol{\eta}) - \tilde{u}_i(\boldsymbol{\xi})]\partial_j \zeta(\frac{\boldsymbol{\eta}-\boldsymbol{\xi}}{\Delta})\, d\boldsymbol{\eta}$$

We now go back to the variables $\mathbf{x} = g^{-1}(\boldsymbol{\xi}), \mathbf{y} = g^{-1}(\boldsymbol{\eta})$ and notice that $\omega d\boldsymbol{\eta} = \Delta^3 d\mathbf{y}$. The additional approximation

$$(\xi_k - \eta_k)\Delta_k(\boldsymbol{\xi}) \simeq (x_k - y_k)\Delta$$

shows that the model (15) is indeed an integral formula for the SGS model

$$\partial_j \tau_{ij} \simeq \partial_j\left(\Delta_k(\mathbf{x})^2 D_{ik}\mathbf{u} D_{jk}\mathbf{u}\right) \tag{17}$$

Another effect of grid refinement is to modify the asymptotic decay rate. Under the assumptions (11), one gets by calculations similar to those in 2.2

$$\mathcal{D}(x_2) \simeq x_2 \Delta_2(x_2)^2 \int |\nabla \mathbf{u}|^2 \, d\mathbf{y}$$

For a Chebyshev grid in the wall normal direction, where $\Delta_2(x_2) \simeq \Delta\sqrt{x_2}$ near the wall, this yields an improved $O(x_2^2)$ decay rate.

An interpretation of the model (17), is that the three eddy-viscosity length scales are given by the grid spacing in the corresponding directions. The implicit additional damping resulting from grid refinement should not be confused with the *ad-hoc* damping sometimes used in conjunction with the Smagorinsky model [12] to improve its effectiveness for wall-bounded flows. If one adopts the view point that LES computations are expected to compute the flow quantities averaged on scales which match the computational grid, we believe that it is natural for a SGS model to eventually reflect the grid geometry. The modification needed in the dissipation tensor is then consistent with the fact that differentiation does not commute with variable size filtering. Moreover, unlike damped Smagorinsky model, the integral formula (15) would easily handle grid refinement in complex geometries, in which case the corresponding differential models can be derived through the appropriate change of variables along the same lines as above.

To evaluate the impact of anisotropic viscous length scales, we have also considered a filter choice for which the resulting dissipation scale in the wall normal direction would be equal to a value $\Delta = (\Delta_1\Delta_2\Delta_3)^{1/3}$ that can be seen as a local mean grid size. The model then reads

$$\sum_j \partial_j \tau_{ij}(\mathbf{x}) \simeq C \frac{\Delta^2(\mathbf{x})}{\Delta_2^2(x_2)} \frac{1}{\omega(\mathbf{x})} \sum_j \frac{1}{\Delta_j(x_j)} \int [u_j(\mathbf{y}) - u_j(\mathbf{x})][u_i(\mathbf{y}) - u_i(\mathbf{x})] \lambda_j(\mathbf{x}, \mathbf{y}) \, d\mathbf{y} \qquad (18)$$

The dissipation scales in the 3 directions will then be respectively $\Delta_1\Delta/\Delta_2$, Δ and $\Delta_3\Delta/\Delta_2$. In the case when $\Delta_2 << \Delta_1 = \Delta_3$, this has the effect of enhancing the dissipation in the

homogeneous directions.

Let us point out that it does not seem possible to derive simple formulas on a variable size grid involving a stencil restricted to the nearest grid point that could give isotropic dissipation scales. Spherical numerical filters would yield isotropic dissipation scales but at the expense of a growing number of discretization points as one gets closer to the boundary. So far, we wanted to avoid the resulting computational overhead. This is however a further option that we plan to investigate in the future.

2.4 Backscatter control

As it has been described so far, our model can clearly produce negative viscosity values. Although this might be seen as a desirable feature, it is well known that persistent negative viscosity can lead to numerical instabilities. The method proposed in [9] to control the backscatter resulting from the model (3), consists in computing the contribution of (3) to the energy balance and damping the subgrid-scale stress when it gives positive contribution. However, both dissipation and backscatter can be expected at a given location along transverse directions (for an incompressible flow, this merely results from the fact that the trace of the tensor $[D_{ij}\mathbf{u}]$ is zero) and the drawback of this method is that it may affect indiscriminatingly the dissipation as well as the backscatter.

By distinguishing among the strain directions, the integral formulation allows a sharper control of the backscatter. Based on the dissipation calculation leading to (10), one can ensure that strict subgrid-scale dissipation can be enforced in (1) by a grid discretization of the following integral model:

$$\partial_j \tau_{ij} \simeq \Delta^{-4} \int \left\{ [\mathbf{u}(\mathbf{x}) - \mathbf{u}(\mathbf{y})] \cdot \nabla \zeta(\frac{\mathbf{x}-\mathbf{y}}{\Delta}) \right\}_+ [\mathbf{u}(\mathbf{x}) - \mathbf{u}(\mathbf{y})]\, d\mathbf{y} \tag{19}$$

where $a_+ = \max(0, a)$. This model can be viewed as a practical mean to evaluate the positive

eigenvalues of the eddy-viscosity tensor, along with the corresponding eigen directions. A similar formula can be derived if one only wishes to prevent the backscatter from exceeding the molecular dissipation. Using the same derivation as in 2.1, this dissipation can be evaluated at a given location $\mathbf{x}$ by

$$\nu\Delta^{-4}\int[\mathbf{u}(\mathbf{x})-\mathbf{u}(\mathbf{y})]^2\zeta(\frac{\mathbf{x}-\mathbf{y}}{\Delta})\,d\mathbf{y}$$

and the corresponding clipping would yield the model

$$\partial_j\tau_{ij}\simeq \tag{20}$$
$$\Delta^{-4}\int\left[\left\{(\mathbf{u}(\mathbf{x})-\mathbf{u}(\mathbf{y}))\cdot\nabla\zeta(\frac{\mathbf{x}-\mathbf{y}}{\Delta})+\nu\zeta(\frac{\mathbf{x}-\mathbf{y}}{\Delta})\right\}_+-\nu\zeta(\frac{\mathbf{x}-\mathbf{y}}{\Delta})\right][\mathbf{u}(\mathbf{x})-\mathbf{u}(\mathbf{y})]\,d\mathbf{y}$$

The models (15) and (18) can easily be modified accordingly. More dissipative variants of these methods would consist in taking absolute values instead of positive values in (19) and (20). In the first case, the stencil in Figure 1 would have to be modified by changing the off-diagonal terms into their absolute values. Under this form, the model can be seen as an anisotropic generalization of the structure-function model of Métais-Lesieur [11]. The anisotropic model is however less dissipative, even in this clipped version. This is easily seen by considering the simple cases of the laminar flow resulting from a shear layer orthogonal to one of the grid axis, or a circular eddy, in which case the dissipation produced by the base anisotropic model (3) and our integral models (8) or (19) would vanish.

2.5 A remark on vortex methods

Vortex methods consist in representing the vorticity field by a distribution of particles carrying local values of the circulation:

$$\boldsymbol{\omega}(\mathbf{x},t)=\sum_p\boldsymbol{\Gamma}_p\delta(\mathbf{x}-\mathbf{x}_p) \tag{21}$$

In 3D incompressible flows, the particles move with the local velocity and their circulations are updated to account for the stretching. The method can be summarized by the following set of differential equations

$$\frac{d\mathbf{x}_p}{dt} = \overline{\mathbf{u}}(\mathbf{x}_p, t) \ , \ \frac{d\mathbf{\Gamma}_p}{dt} = \nabla\overline{\mathbf{u}}(\mathbf{x}_p, t)\mathbf{\Gamma}_p$$

In the above equations $\overline{\mathbf{u}}$ represents the velocity computed through a regularized Biot-Savart equation. The particle vorticity field given by (21) can then be proved to solve *exactly* the equation:

$$\frac{\partial \omega_i}{\partial t} + \text{div}\,\{\overline{\mathbf{u}}\omega_i\} - \text{div}\,\{\boldsymbol{\omega}\overline{u}_i\} = 0 \tag{22}$$

A continuous vorticity field is generally recovered by considering vortex blobs obtained from the particles through filtering with a cut-off function. The same filtering operation is performed before using the Biot-Savart law to compute the velocity. As it results from (21), the vortex-blob field satisfies

$$\frac{\partial \overline{\boldsymbol{\omega}}_i}{\partial t} + \text{div}\,\{\overline{\overline{\mathbf{u}}\boldsymbol{\omega}_i}\} - \text{div}\,\{\overline{\boldsymbol{\omega}\overline{u}_i}\} = 0 \tag{23}$$

In other words, up to the change of $\mathbf{u}$ into $\overline{\mathbf{u}}$, vortex methods solve the filtered Euler equations. This feature strikingly distinguishes these methods from Eulerian methods. It implies that, if one relies on the subgrid-scale model

$$\overline{\overline{u}_i\omega_j} - \overline{u}_i\overline{\omega}_j \simeq C\Delta^2 \sum_{k=1}^{3} D_{ik}\overline{\mathbf{u}}D_{jk}\overline{\boldsymbol{\omega}} \tag{24}$$

vortex methods incorporate both the backscatter and the dissipation induced by the right hand side of (24). In [2] a correction scheme was designed to selectively remove the backscatter contribution of the subgrid-scales and tested in two-dimensional turbulence. The extension to three-dimensional flows of this algorithm reads

$$\frac{d\mathbf{\Gamma}_p}{dt} = \nabla\overline{\mathbf{u}}(\mathbf{x}_p, t)\mathbf{\Gamma}_p + \Delta^{-4}\sum_q v_q \left\{[\mathbf{u}(\mathbf{x}_p) - \mathbf{u}(\mathbf{x}_q)]\cdot\nabla\zeta(\frac{\mathbf{x}_p - \mathbf{x}_q}{\Delta})\right\}_{-}[\mathbf{\Gamma}_p - \mathbf{\Gamma}_q]$$

where v_q denote the volumes of the particles. In the light of the preceding discussion, one may interpret this scheme as an integral formula, on a lagrangian grid, to remove part of the enstrophy backscatter resulting from the subgrid-scale stress (24) implicitly involved in the vortex scheme (23).

2.6 Dynamic procedure

In the case of a uniform grid, the dynamic calculation of the model coefficient can be done along the same lines as for the Smagorinsky model, on the basis of the approximation (6).

We classically denote by $\overline{()}, \widehat{()}$ filtering at scales Δ and 2Δ, and by τ_{ij}, T_{ij} the subgrid stresses at the corresponding scales. We start from the following algebraic identity

$$L_{ij} = T_{ij} - \hat{\tau}_{ij} \tag{25}$$

where

$$L_{ij} = \widehat{\bar{u}_i \bar{u}_j} - \hat{\bar{u}}_i \hat{\bar{u}}_j \ , T_{ij} = \widehat{\overline{u_i u_j}} - \hat{\bar{u}}_i \hat{\bar{u}}_j \ , \hat{\tau}_{ij} = \widehat{\overline{u_i u_j}} - \widehat{\bar{u}_i \bar{u}_j}$$

L_{ij} can be evaluated from the computed grid values u_i, whereas T_{ij} and τ_{ij} are modeled through (6). (25) results then in a system of 6 integral equations in the unknown coefficient C. If one assumes that C does not vary on filter scales, one can then bring it out of the integrals and solve the resulting equations in the least square sense. The same procedure can be followed for a non-uniform mesh, starting from (14) instead of (6).

Obviously, the validity of the above procedure is strongly conditioned by the consistency of the assumption that the variations of C are small on filter scales. The claim is that the anisotropic form (3) is better conditioned than the Smagorinsky model to make such an assumption reasonable. The subgrid-scale dissipation curves that we will show in the next section, obtained with constant coefficients, seem to substantiate this claim.

3 Numerical Results

Our numerical experiments have focused on channel calculations at a Reynolds number of $Re_\tau = 1,030$ based on the shear velocity, which corresponds to a Reynolds number of about $25,000$ based on the centerline velocity and the channel half-width, which will be taken as 1 in our calculations. The computational grid used respectively $48, 73$ and 64 points in the streamwise, transverse and spanwise directions, for a channel of size $2\pi \times 2 \times 3\pi/4$. The velocity components in the streamwise, transverse and spanwise directions, along with the corresponding coordinates, will be respectively denoted by u, v, w, and x, y, z. As it is customary, we will also use the transverse coordinates in wall-units defined by $y_+ = y/Re_\tau$.

Our model was implemented in a Chebyshev-Fourier collocation code [7]. In this numerical scheme, the Crank Nicolson time-advancing scheme is used for the diffusion equation in the wall normal direction together with a third order Runge Kutta method to account for the non linear convection and SGS terms. Periodic boundary conditions are assumed in the streamwise and spanwise directions, and no-slip conditions at the walls located at $y = \pm 1$. Dealiasing is performed in the periodic directions and the pressure is updated at each iteration to maintain a constant momentum throughout the calculation.

We will compare our model with dynamic model results as well as the experiments reported in [16]. The dynamic model we used is described in [5]. It is a global, plane-averaged, dynamic model based on (25), with top-hat filtering on the scale 2Δ along the streamwise and spanwise direction. The model coefficient is computed through a least-square procedure and then averaged in the homogeneous directions of the flow. For the implementation of our model we have chosen a filter consisting in the tensor product of quadratic B-splines with support containing

three grid points. Three different options of our model have been implemented:

case 1: scaling (18) and no-clipping, $C = .01$

case 2: scaling (15) and no-clipping, $C = .25$

case 3: scaling (15) and clipping (20), $C = .075$

Note that, while the constant used for case 1 is in the same order of magnitude as the one usually used for Smagorinsky model, for the the other cases, in particular case 2, it is significantly higher.

To immediately give an idea of the dissipation produced by the various models, we compared the SGS dissipation obtained through our model with that of the dynamic model. We computed the dissipations for the turbulent field that we used as initial condition in all our experiments. The results are shown in the vicinity of the wall in Figure 2. One first observation is that all models produce dissipation in the same order of magnitude (note that the dissipation of the Smagorinsky model with constant .01 would go off the chart). This is actually on the basis of such curves that we have roughly adjusted the various constants in our cases. The dissipation profiles obtained by the dynamic model and our cases 2 and 3 are strikingly similar. This fact raises some hope that the dynamic procedure outlined above will not lead to highly oscillatory coefficient values. Notice that Case 1 differs from the others by a much more localized dissipation in the near wall region.

Figure 3 shows the mean velocity profiles obtained by the various methods, as well as the theoretical logarithmic curve for the central part of the channel as functions of the distance to the walls in wall-units. All methods give comparable results (in particular they all fail to be very accurate at this grid resolution in the logarithmic zone). However Case 1 seems to give

the best results in this zone, while cases 2 and 3 somewhat underestimate the velocity in the near wall region.

Let us now turn to second order statistics. The turbulence intensities in our cases are compared in Figure 4 with the dynamic model and experimental results from [16] corresponding to a Reynolds number of $22,776$. Cases 2 and 3 give results that are very close to the dynamic model. As for Case 1, it seems to give in the center of the channel results which would correspond to a higher value of the Reynolds number. This might be related to the observation we already made on the fact that the SGS dissipation is very much concentrated near the walls and suggests that, for the chosen value of the coefficient, the model is not dissipating enough in the center of the channel.

The large scale shear stress $\overline{uv}$ is shown on Figure 5. In the near wall region, the slopes of the curves obtained by the various models are very similar, while Cases 2 and 3 slightly underpredict the shear stress in the intermediate region for $60 < y_+ < 100$. As a last test, we show in Figure 6 the 2 point correlations in the spanwise direction obtained by the various models at a distance from the wall of about 15 wall units. Cases 2 and 3 give negative correlations for the streamwise component that indicate better than the dynamic model the presence of streaks of adverse velocities in the boundary layer. As for case 1, it gives results similar to the dynamic model. The inferior performance of Case 1 in this last test, compared to cases 2 and 3, can probably be accounted for by the fact that, by construction, this model produces excessive dissipation in the homogeneous directions.

4 Summary and conclusion

We have derived a numerical method related to a subgrid-scale model using an eddy-viscosity tensor. Strict dissipation can be enforced by appropriate clipping procedures which are able to distinguish among the strain directions of the flow. Depending on how it is implemented, the model can allow grid refinement to translate into anisotropic subgrid viscous length scales and improved decay rates near walls. From the numerical results presented, these options do not seem to have a crucial effect; the modification of the viscous scales in the wall normal direction can essentially be compensated by a proper choice of the model coefficient. One can expect that a dynamic computation of the coefficient would further reduce the influence of the particular model implemented. The model where the dissipation scales adjust to the grid and its clipped version seem, by their simplicity, good candidates to carry on to more general geometries. Together with the implementation of the dynamic procedure, this will be addressed in future works. We also plan to test for isotropic turbulence cases hyperviscosity models using filters with vanishing second order momentum.

Acknowledgements

I wish to thank P. Moin and N. Mansour for their hospitality during the preparation of this paper. Helpful discussions with W. Cabot, P. Koumoutsakos and K. Shariff are also gratefully acknowledged. Computer time was provided by NASA Ames Supercomputing Center.

References

[1] W. Cabot, *Local dynamic subgrid-scale models in channel flow*, Annual Research Briefs, Center for Turbulence Research, Stanford, 1994

[2] G.-H. Cottet, *Artificial viscosity models for vortex and particle methods*, J. Comp. Physics, **127**, 299-308, 1996

[3] G-H. Cottet and A.A Wray, *Anisotropic grid-based formulas for subgrid-scale models*, Annual Research Briefs, Center for Turbulence Research, 113-122, 1997

[4] P. Degond and S. Mas-Gallic, *The weighted particle method for convection-diffusion equations*, Math. Comp., **53**, 485-526, 1989

[5] M. Germano, U. Piomelli, P. Moin and W.H. Cabot, *A dynamic subgrid-scale eddy viscosity model*, Phys. Fluids A, **3**, 1760-1765, 1991

[6] S. Ghosal, T.S. Lund, P. Moin and K. Akselvoll, *A dynamic localization model for large-eddy simulation of turbulent flow*, J. Fluid. Mech., **286**, 229-255, 1995

[7] J. Kim, P. Moin and R. Moser, *Turbulence statistics in fully developed channel flow at low Reynolds number*, J. Fluid Mech., **177**, 133-166, 1987

[8] A. Leonard, *Energy cascade in large-eddy simulations of turbulent fluid flows*, Adv. Geophys., **18**, 237-248, 1974

[9] S. Liu, C. Meneveau and J. Katz, *The property of similarity subgrid-scale models*, J. Fluid Mech., **275**, 83-119, 1994

[10] T.S. Lund and E.A. Novikov, *Parametrization of subgrid-scale stress by the velocity gradient tensor*, Annual Research Briefs, Center for Turbulence Research, Stanford, 1992

[11] O. Métais and M. Lesieur, *Spectral large-eddy simulation of isotropic and stably-stratified turbulence*, J. Fluid Mech., **39**, 157-194, 1992

[12] U. Piomelli, T.A. Zhang, C.G. Speziale and Y. Hussaini, *On the large-eddy simulation of transitional wall-bounded flows*, Phys. Fluids A, **2**, 257-265, 1990

[13] U. Piomelli and J. Liu, *Large-eddy simulations of rotating channel flows using a localized dynamic model*, Phys. Fluids, **7**, 839-848, 1995

[14] J. Smagorinsky, *General circulation experiments with the primitive equations*, Mon. Weather Rev, **91**, 99-164, 1963

[15] V. Vreman, B. Geurts and H. Kuerten, *Large-eddy simulations of the turbulent mixing layer*, J. Fluid Mech., **339**, 357-390, 1997

[16] T. Wei and W. Willmarth, *Reynolds number effects on turbulent channel flows*, J. Fluid Mech., **204**, 57, 1989

Figure captions

Figure 1. Finite-difference stencil of the subgrid-scale model in the case of a uniform grid with a radial hat filter. $\alpha_T/\Delta, \alpha_E/\Delta, \cdots$ denote the weights of the corresponding grid points.

Figure 2. SGS dissipation for the dynamic model (DM) and cases 1 to 3.

Figure 3. Mean velocity profiles for the dynamic model (DM) and cases 1 to 3.

Figure 4. Turbulence intensities in wall coordinates; top curves: streamwise velocity, middle curves: normal velocity, bottom curves: spanwise velocity.

Figure 5. Large Scale shear stress in wall coordinates.

Figure 6. Spanwise two point correlations at $Y_+ \simeq 15$. Top picture: streamwise velocity, bottom picture: transverse velocity.

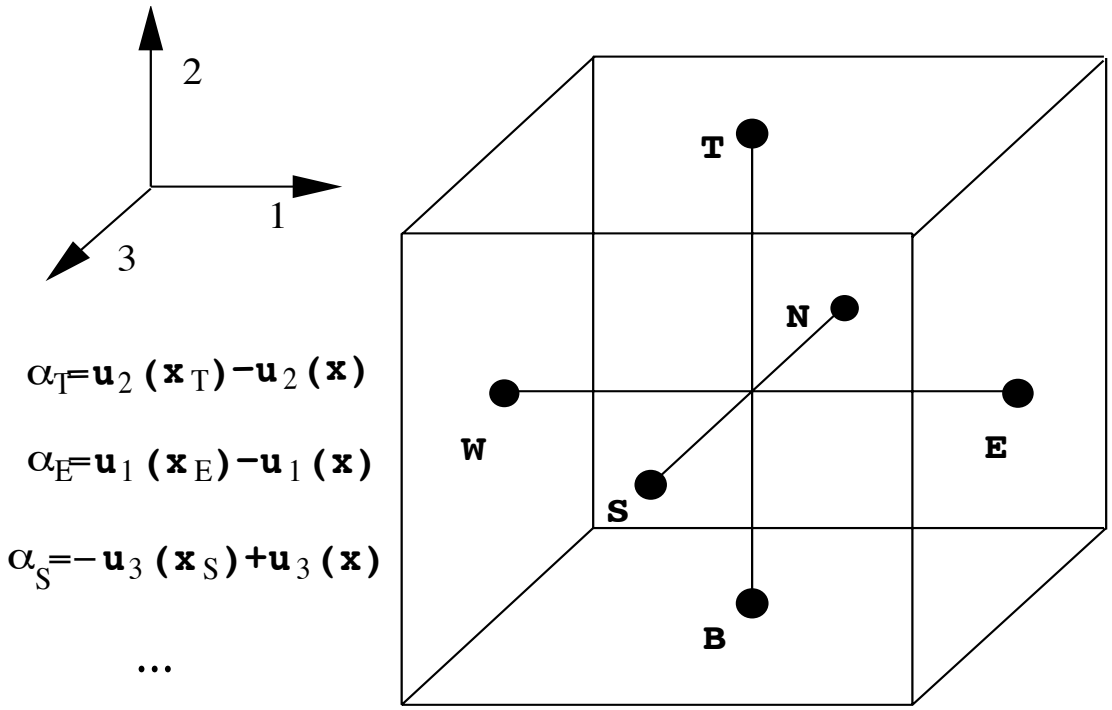

Figure 1: Finite-difference stencil of the subgrid-scale model in the case of a uniform grid with a radial hat filter. $\alpha_T/\Delta, \alpha_E/\Delta, \cdots$ denote the weights of the corresponding grid points.

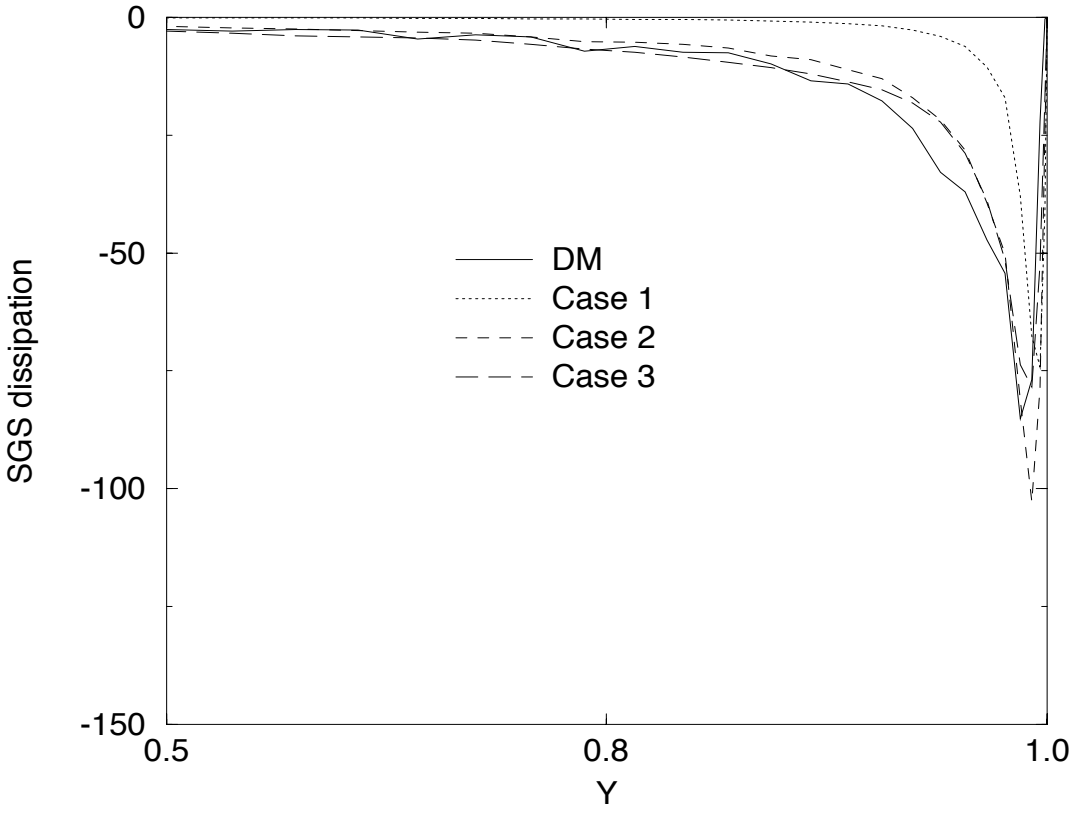

Figure 2: SGS dissipation for the dynamic model (DM) and cases 1 to 3

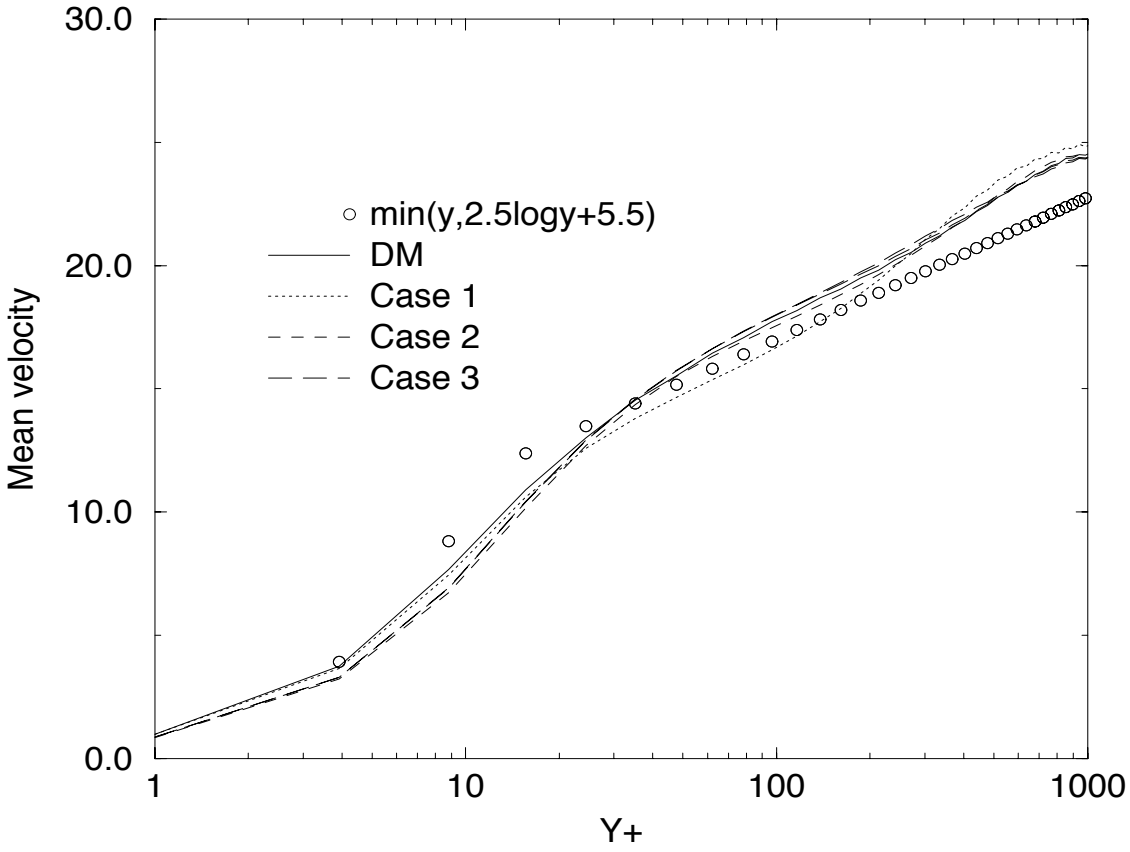

Figure 3: Mean velocity profiles for the dynamic model (DM) and cases 1 to 3

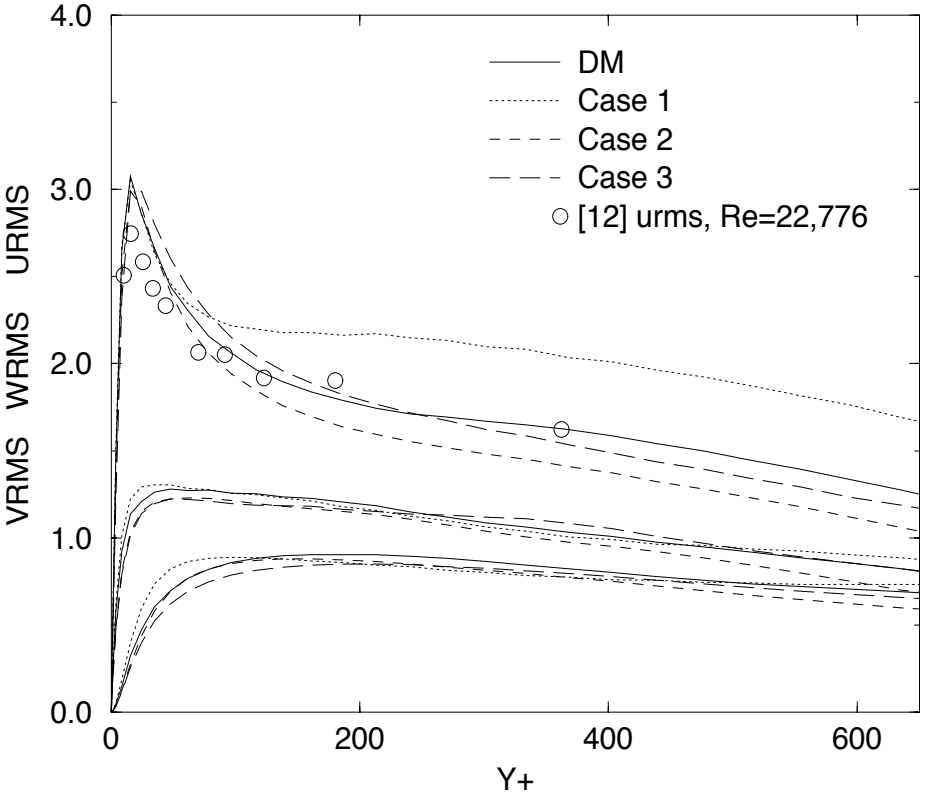

Figure 4: Turbulence intensities in wall coordinates; top curves: streamwise velocity, middle curves: normal velocity, bottom curves: spanwise velocity.

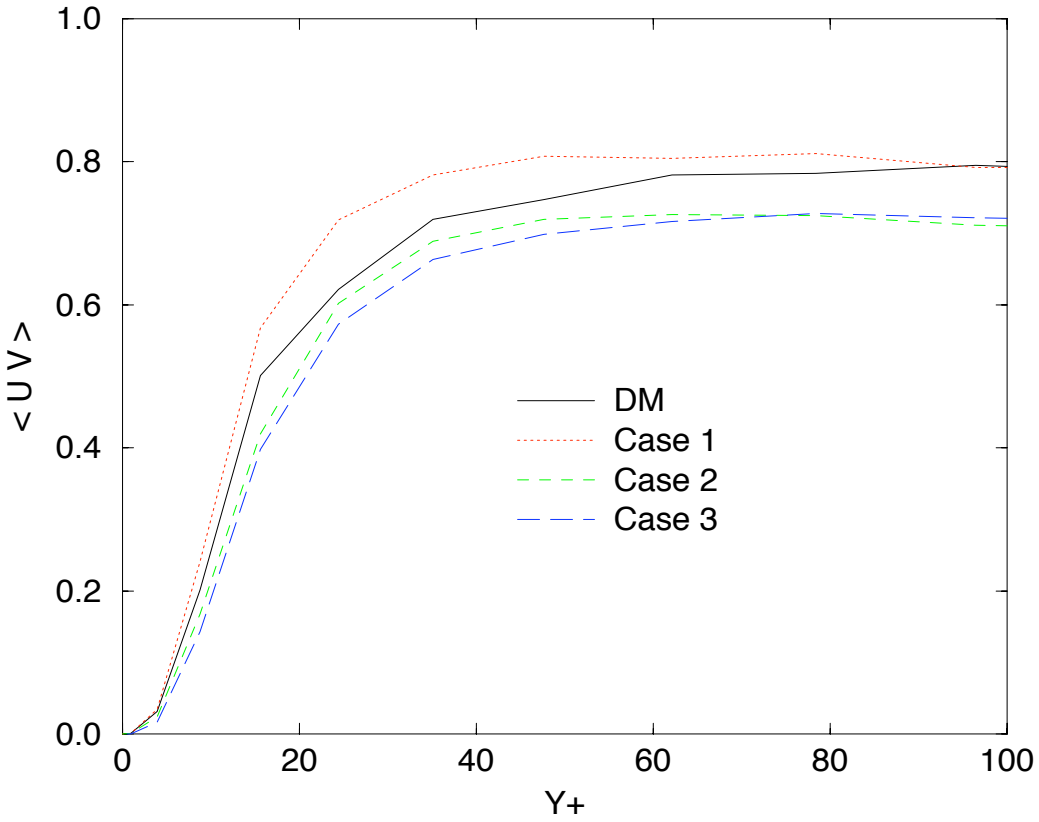

Figure 5: Large Scale shear stress in wall coordinates

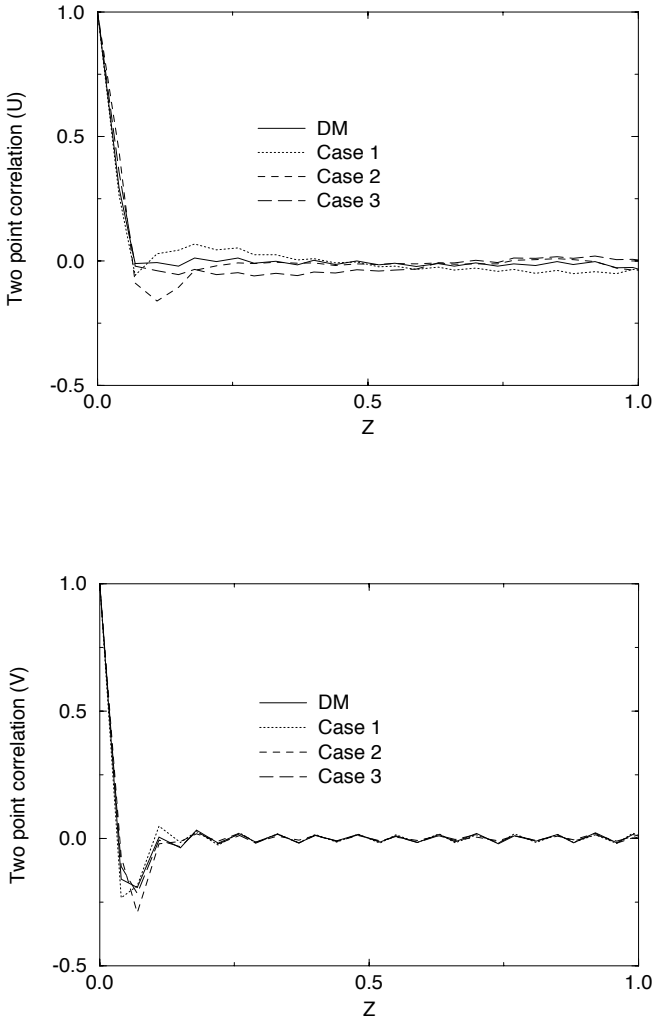

Figure 6: Spanwise two point correlations at $Y_+ \simeq 15$. Top picture: streamwise velocity, bottom picture: transverse velocity